Article

Cell Reports

Repression of the Central Splicing Regulator RBFox2 Is Functionally Linked to Pressure Overload-Induced Heart Failure

Graphical Abstract

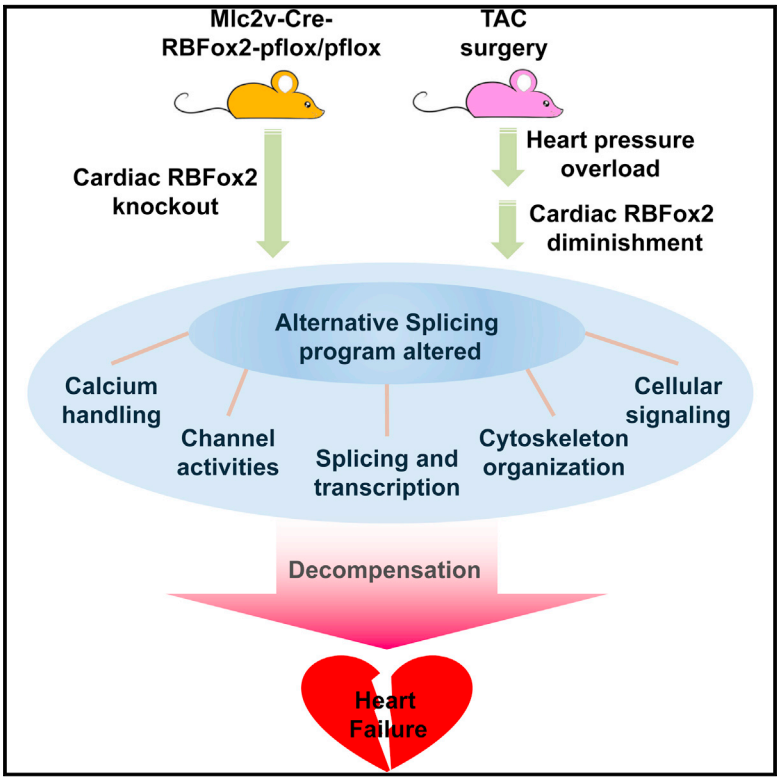

Authors

Chaoliang Wei, Jinsong Qiu, ..., Long-Sheng Song, Xiang-Dong Fu

Correspondence

xdfu@ucsd.edu

In Brief

Wei et al. report that RBFox2 functions as a key splicing regulator during postnatal heart remodeling, and tissue-specific ablation of *RBFox2* in the heart causes lethal dilated cardiomyopathy. RBFox2 protein is potently decreased in a heart failure model induced by transverse aortic constriction, suggesting RBFox2 is a key stress sensor in the heart.

Highlights

- Pressure overloading the mouse heart decreases RBFox2 protein
- Pressure overload and cardiac ablation of RBFox2 induce similar heart failure
- RBFox2 regulates a large splicing program important for heart function
- Data suggest RBFox2 is a key stress sensor in heart disease

Accession Numbers

GSE57926

Wei et al., 2015, Cell Reports *10*, 1521–1533
March 10, 2015
http://dx.doi.org/10.1016/j.celrep.2015.02.013

Cell Reports
Article

Repression of the Central Splicing Regulator RBFox2 Is Functionally Linked to Pressure Overload-Induced Heart Failure

Chaoliang Wei,[1] Jinsong Qiu,[1] Yu Zhou,[1] Yuanchao Xue,[1] Jing Hu,[1] Kunfu Ouyang,[2] Indroneal Banerjee,[2] Caimei Zhang,[4] Biyi Chen,[4] Hairi Li,[1] Ju Chen,[2] Long-Sheng Song,[4] and Xiang-Dong Fu[1,3,*]
[1]Department of Cellular and Molecular Medicine University of California, San Diego, La Jolla, CA 92093-0651, USA
[2]Department of Medicine University of California, San Diego, La Jolla, CA 92093-0651, USA
[3]Institute of Genomic Medicine, University of California, San Diego, La Jolla, CA 92093-0651, USA
[4]Division of Cardiovascular Medicine, Department of Internal Medicine, University of Iowa Carver College of Medicine, Iowa City, IA 52242, USA
*Correspondence: xdfu@ucsd.edu
http://dx.doi.org/10.1016/j.celrep.2015.02.013

SUMMARY

Heart failure is characterized by the transition from an initial compensatory response to decompensation, which can be partially mimicked by transverse aortic constriction (TAC) in rodent models. Numerous signaling molecules have been shown to be part of the compensatory program, but relatively little is known about the transition to decompensation that leads to heart failure. Here, we show that TAC potently decreases the RBFox2 protein in the mouse heart, and cardiac ablation of this critical splicing regulator generates many phenotypes resembling those associated with decompensation in the failing heart. Global analysis reveals that RBFox2 regulates splicing of many genes implicated in heart function and disease. A subset of these genes undergoes developmental regulation during postnatal heart remodeling, which is reversed in TAC-treated and *RBFox2* knockout mice. These findings suggest that RBFox2 may be a critical stress sensor during pressure overload-induced heart failure.

INTRODUCTION

The mammalian heart contains post-mitotic cardiomyocytes, and pathological loss of these cells is the ultimate cause of heart failure (Diwan and Dorn, 2007). Most forms of cardiomyopathy are associated with initial cardiac hypertrophy, which has been widely considered a compensatory program during pathological conditions. However, hypertrophy per se is not a prerequisite for heart failure, as it also occurs under physiological conditions (e.g., exercise). Even under pathological conditions (i.e., hypertension, myocardial infarction, or ischemia), hypertrophy can be decoupled from functional compensation in various genetic models (Hill et al., 2000). Instead, progression to heart failure is linked to the so-called decompensation process, which leads to myocardial insufficiency (Diwan and Dorn, 2007). The induction of several critical signaling pathways has been linked to the compensatory program, some of which appear to also contribute to decompensation (Marber et al., 2011). However, relatively little is known about molecular events responsible for the transition from compensation to decompensation. In fact, global approaches have been applied to heart disease samples from both humans and animals (Giudice et al., 2014; Kaynak et al., 2003), but it remains unclear whether dysregulation of individual genes are a cause or consequence of heart failure.

The RBFox family of RNA-binding proteins has been implicated in development and disease (Kuroyanagi, 2009). Mammalian genomes encode three RBFox family members, all of which show prevalent expression in the brain. RBFox1 (A2BP1) and RBFox2 (RMB9 or Fxh) are known to play central roles in brain development (Gehman et al., 2011, 2012), whereas RBFox3 (NeuN) is a well-established biomarker for mature neurons (Kim et al., 2009). In addition, both *RBFox1* and *RBFox2* are expressed in the heart where *RBFox2* is expressed from embryo to adult and *RBFox1* is induced in postnatal heart (Kalsotra et al., 2008), contributing to heart development and function in zebrafish (Gallagher et al., 2011). Upregulation of *RBFox1* has been detected in the failing heart in humans (Kaynak et al., 2003), whereas mutations in *RBFox2* have been linked to various human diseases, including autism (Sebat et al., 2007) and cancer (Venables et al., 2009). A more recent study demonstrated that RBFox2, but not RBFox1, is required for myoblast fusion during C2C12 cell differentiation (Singh et al., 2014), thus strongly implicating RBFox2 in heart development and function in mammals. At the molecular level, both RBFox1 and RBFox2 have been extensively characterized as splicing regulators that recognize the evolutionarily conserved UGCAUG motif in pre-mRNAs (Zhang et al., 2008) and regulate alternative splicing in a position-dependent manner (Yeo et al., 2009).

Here, we report that the RBFox2 protein is decreased in response to transverse aortic constriction (TAC) in the mouse heart, and cardiac-specific ablation of *RBFox2* generates an array of phenotypes resembling those in TAC-induced heart failure. Global analysis reveals an extensive RBFox2-regulated splicing

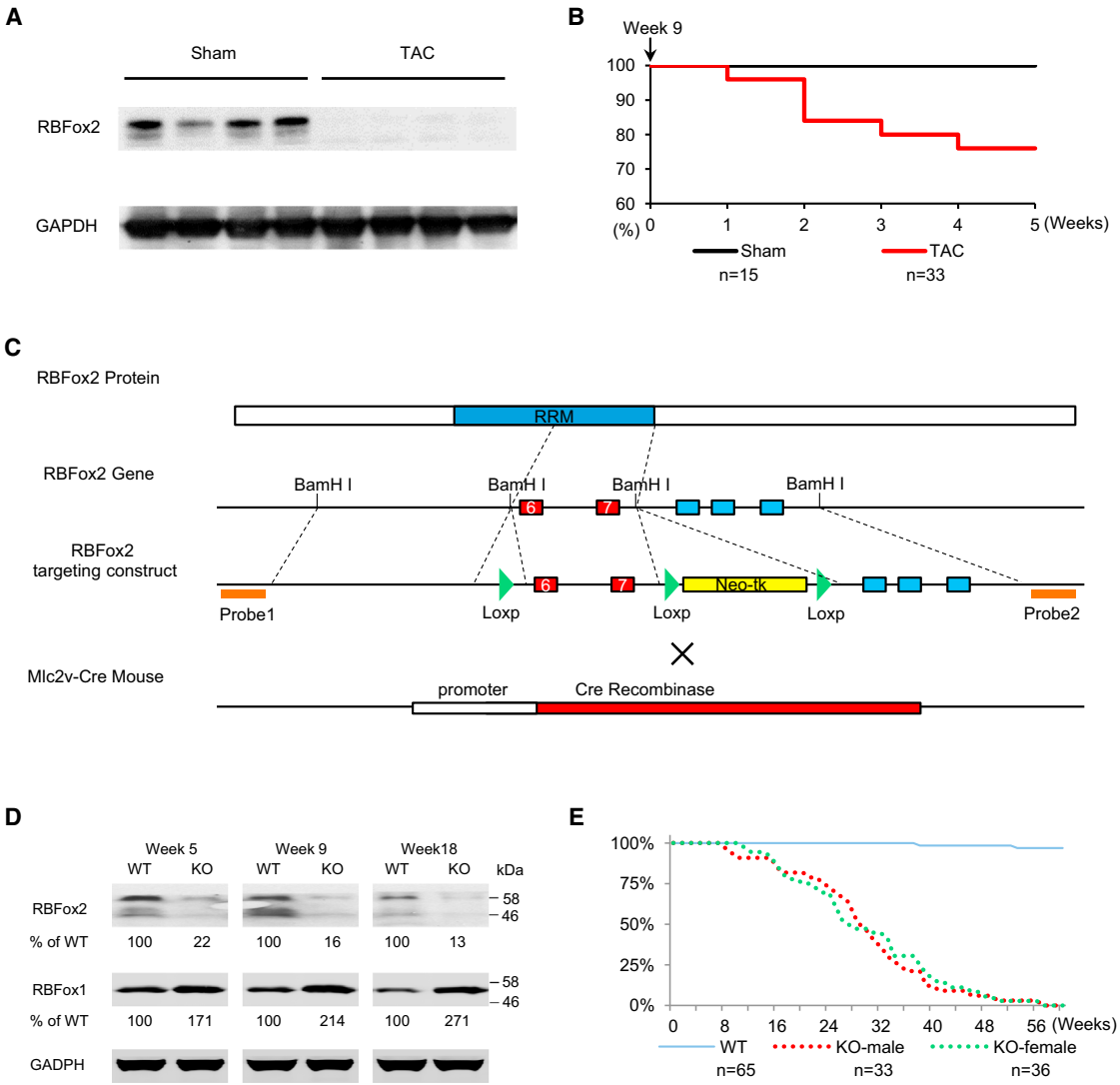

Figure 1. Essential Requirement for RBFox2 to Prevent Heart Failure

(A) Western blotting analysis of RBFox2 in sham- and TAC-treated mice after 5 weeks postsurgery. GADPH served as a loading control.

(B) Kaplan-Meier survival curves of sham and TAC littermate male mice.

(C) Conditional *RBFox2* KO and generation of heart-specific KO by crossing with an *Mlc2v-Cre* transgenic mouse.

(D) Western blotting analysis of RBFox1 and RBFox2 in WT and *RBFox2* KO cardiomyocytes at three postnatal stages. Triplicate results were quantified relative to WT, as indicated below each gel.

(E) Survival curves of WT and *RBFox2* KO littermate mice in both sexes.

program, which likely constitutes a key part of the developmental program during postnatal heart remodeling, and, importantly, both TAC treatment and *RBFox2* ablation reverse this splicing program. These findings suggest that diminished RBFox2 expression may be a key event during heart decompensation.

RESULTS

RBFox2 Is Functionally Linked to Pressure Overload-Induced Heart Failure

RBFox2 shows prevalent expression throughout heart development (Kalsotra et al., 2008), but its biological function in cardiac muscle and potential contribution to heart disease in mammals have remained unexplored. We first tested whether RBFox2 expression might be perturbed in a TAC-induced heart failure model. Strikingly, we found that RBFox2 protein was largely diminished in the heart of live mice 5 weeks after TAC (Figure 1A), which resulted in ~30% mortality (Figure 1B). These data suggest that RBFox2 may function as a key sensor to cardiac stress and its downregulation is linked to heart failure.

To determine whether RBFox2 has a potential to contribute to, rather than be a functional consequence of, heart failure, we took advantage of an *RBFox2* conditional knockout (KO) mouse (Gehman et al., 2012). By crossing *RBFox2*$^{f/f}$ mice with an *Mlc2v-Cre*

(active at E8.5) transgenic mouse (Chen et al., 1998), we ablated the gene at the onset of cardiogenesis (Figure 1C). Mice with different genotypes all gave live birth, indicating that, once the cardiogenic program is launched, *RBFox2* is not essential for the remaining steps in organ formation throughout embryonic development.

Western blotting showed that the RBFox2 protein was substantially reduced in isolated *RBFox2*$^{-/-}$ cardiomyocytes at the several postnatal stages we examined (Figure 1D). In comparison, RBFox1 was elevated to some extent in *RBFox2*$^{-/-}$ hearts, indicating a degree of functional compensation. However, RBFox2 clearly has a unique functional requirement in the heart, as less than 5% of *RBFox2*-ablated mice of both sexes were able to survive beyond 1 year (Figure 1E). These results establish an essential function of RBFox2 in postnatal heart, and, importantly, suggest that diminished RBFox2 may be functionally linked to pressure overload-induced heart failure.

RBFox2 Ablation Causes Dilated Cardiomyopathy that Leads to Heart Failure

By echocardiography, we recorded severe contraction defects in *RBFox2*$^{-/-}$ heart (Figures 2A and S1A), which is characterized by a significant increase in both end-systolic and end-diastolic left ventricular internal dimension (LVID-S and LVID-D), resulting in progressive decrease in fractional shortening with age (Figures 2B and S1A). At week 5, both the gross morphology and structure of the *RBFox2*$^{-/-}$ heart showed relatively minor defects (Figures 2C and S1B), but by 9 weeks the cardiac chamber began to enlarge and the ventricular wall became thinner, and by 22 weeks the *RBFox2*$^{-/-}$ heart developed typical dilated cardiomyopathy (DCM) (Figure 2C). Intriguingly, the development of DCM in *RBFox2*$^{-/-}$ mice was not accompanied by the advent of cardiac hypertrophy, as indicated by heart/body ratios similar to wild-type (WT) mice (Figure 2D) and by little increase in cell surface area of cardiomyocytes isolated by enzymatic perfusion at week 9 (Figure 2E). These observations imply that dysregulated RBFox2 may selectively contribute to heart decompensation without first inducing hypertrophy. H&E staining showed extensive disconnection of cardiomyocytes and Trichrome staining revealed increased fibrosis at week 9 and onward (Figures S1B, 2F, and 2G).

Next, we examined calcium-handling properties on isolated *RBFox2*$^{-/-}$ cardiomyocytes. High-resolution line-scan mode confocal microcopy revealed weakened calcium transients (Figures 3A and 3B), resulting in impaired whole-cell twitch (Figure 3C), even though the sarcoplasmic reticulum (SR) content remained unaltered (Figure S2A). The calcium-handling defect also was reflected by a significant elevation of self-evoked calcium sparks (Figures 3D and 3E), indicative of severe calcium leak (Cheng and Lederer, 2008). To further establish the primary effects, we used two independent small interfering RNAs (siRNAs) to knock down *RBFox2* on cultured neonatal cardiomyocytes from WT mice (Figure S2B), and observed similar calcium-handling defects (Figure S2C), including reduced transient peak (Figure S2D), increased calcium sparks (Figure S2E), and elevated spontaneous transient frequency (Figure S2F). These results suggest a direct contribution of RBFox2 to excitation-contraction (EC) coupling in cardiac muscle.

RBFox2 Regulates a Large Splicing Program in Cardiac Muscle

Given that RBFox2 is a well-established splicing regulator, we next aimed to elucidate the mechanism underlying the observed functional defects by profiling the splicing program perturbed in *RBFox2*$^{-/-}$ heart. We took advantage of the RNA annealing-selection-ligation coupled with deep sequencing (RASL-seq) platform developed in our lab (Zhou et al., 2012), which measures 3,884 annotated alternative splicing events in the mouse genome, thus providing a sensitive and cost-effective means to broadly survey RBFox2-regulated splicing. To distinguish between likely direct functional consequences and those additionally altered by accumulating defects, we surveyed three specific developmental stages at postnatal weeks 5, 9, and 18 in triplicate (Figures 4A and S3A), which respectively represented an initial stage that showed detectable but minimal pathology, an intermediate stage associated with evident cardiac malfunction, and a late stage when KO mice began to die (see Figures 1 and 2).

We recorded a sufficient number of splicing changes (more than ten counts with both isoforms, $p < 0.05$ among triplicate) among ~70% of total surveyed splicing events in both WT and *RBFox2*$^{-/-}$ hearts at all three stages (Figure S3B). In aggregate, we detected a total of 709 splicing switching events in 624 genes, among which 346 events exhibited enhanced exon skipping and 363 events displayed induced exon inclusion in response to *RBFox2* ablation (Figure 4A; Table S2). We noted that the number of dysregulated splicing events was already comparable to that identified by large-scale RNA sequencing (RNA-seq) on *RBFox2* siRNA-treated C2C12 cells (Singh et al., 2014), even though our platform only surveys a set of annotated splicing events. Interestingly, the number of altered splicing events increased during DCM progression: using a stringent cutoff (>2-fold in ratio change in addition to $p < 0.05$), we identified 308 (43.4% of total), 390 (55.0%), and 437 (61.6%) altered splicing events at weeks 5, 9, and 18, respectively (Figures 4B and S3A; Table S2). Together, these findings reveal an extensive splicing program regulated by RBFox2 in the mouse heart.

Context-Dependent RBFox2 Binding Is Responsible for Early Induced Splicing Events

The splicing changes detected at week 5 are likely direct targets because of minimal morphological and structural changes detected at this stage. One effective way to identify direct RBFox2 targets is to determine RBFox2 binding events on induced alternative splicing events and link RBFox2 binding to functional consequences based on its well-established position-dependent effects. We therefore performed genome-wide analysis of RBFox2-RNA interactions by crosslinking iummunoprecipitation followed by deep sequencing (CLIP-seq) on primary cardiomyocytes isolated from WT mice. From 67 million mapped reads and after removing PCR products based on built-in barcodes, we obtained ~15 million CLIP-seq reads that were uniquely mapped to the mouse genome (Figure S3C). Interestingly, 64.0% reads were mapped to intergenic regions, indicating additional functions of RBFox2 in the mouse genome, and 24.3% reads to intron regions, consistent with its roles in regulated splicing (Figure 4C). The RBFox2 CLIP-seq reads were enriched with the

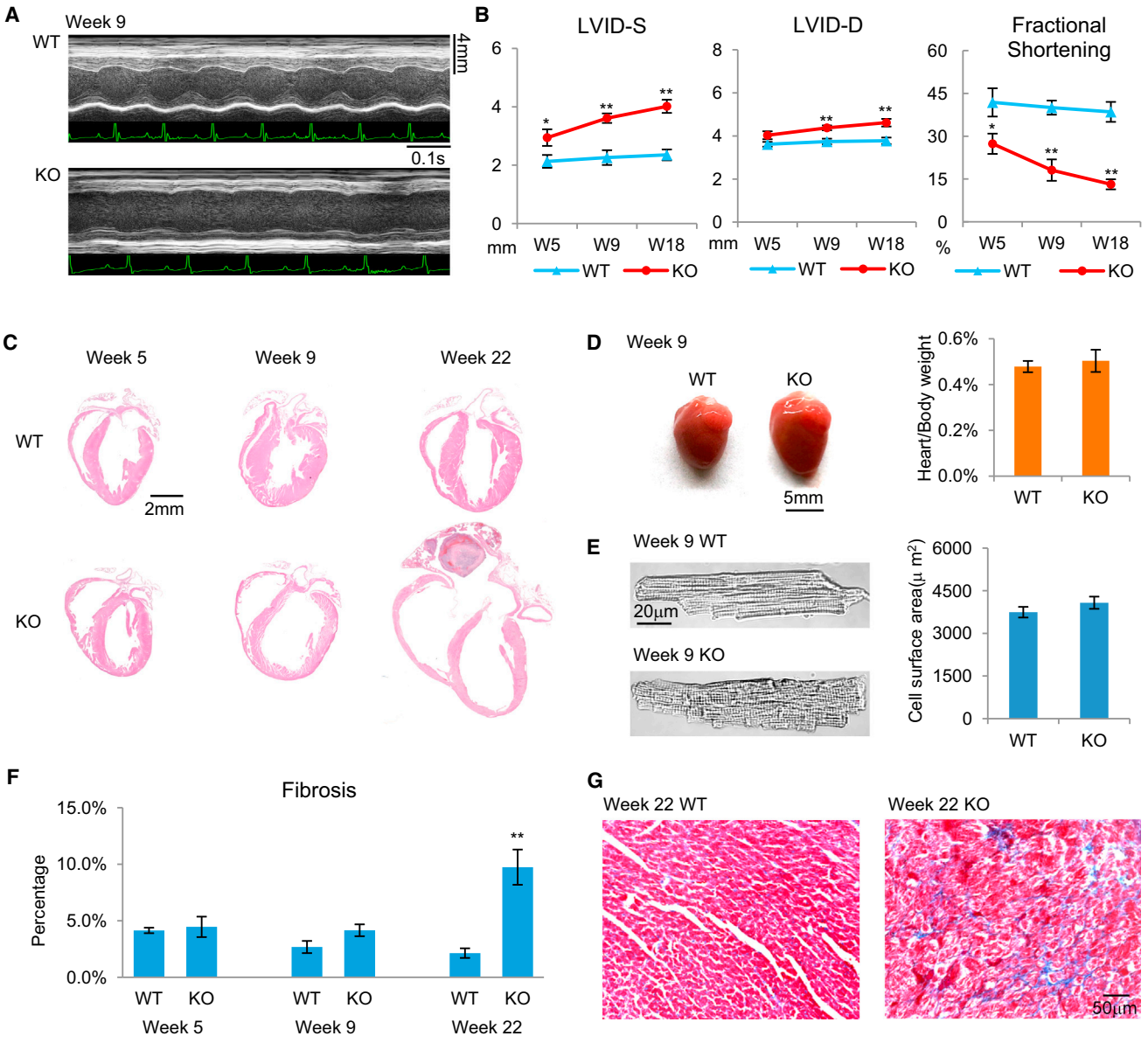

Figure 2. General Heart Failure Phenotype Induced in RBFox2 KO Mice

(A) Examples of cardiac echocardiography of WT and *RBFox2* KO mice acquired at 9 weeks of age.

(B) Key echocardiography parameters of WT and *RBFox2* KO mice at different ages. The data in each group were collected from five to eight mice and expressed as mean ± SEM. *p < 0.05; **p < 0.01.

(C) H&E staining of the coronal sections of WT and *RBFox2* KO hearts at different ages.

(D) Size and mass of WT and *RBFox2* KO hearts at 9 weeks of age. (Left) Side-by-side comparison between WT and KO hearts at 9 weeks. (Right) Statistics of the heart-to-body weight ratio of WT and KO hearts. The data in each group were collected from three mice and expressed as mean ± SEM.

(E) Size of cardiomyocytes isolated from WT and *RBFox2* KO hearts at 9 weeks of age. (Left) Transmission images of WT and *RBFox2*-deleted cardiomyocytes. (Right) Statistics of the cell surface area of WT and KO cardiomyocytes. The data in each group were based on the analysis of 23–25 cells from three mouse hearts and expressed as mean ± SEM.

(F) Statistics of fibrosis from Trichrome-stained WT or *RBFox2* KO hearts at different developmental stages. The data in each group were based on the analysis of five to six images from two mice and expressed as mean ± SEM. **p < 0.01.

(G) Trichrome staining for fibrosis and myofibril disorder in *RBFox2* KO heart by 22 weeks. See also Figure S1.

expected UGCAUG motif (Figures 4C and S3D), which underlies ~29% of 149,832 identified RBFox2 binding peaks (Figure 4C), similar to our previous observation on embryonic stem cells (Yeo et al., 2009).

Next, we linked the CLIP-seq data to regulated splicing events detected by RASL-seq, and observed the expected positional effects on significantly altered events detected at all three stages, showing enhanced exon inclusion when RBFox2 bound

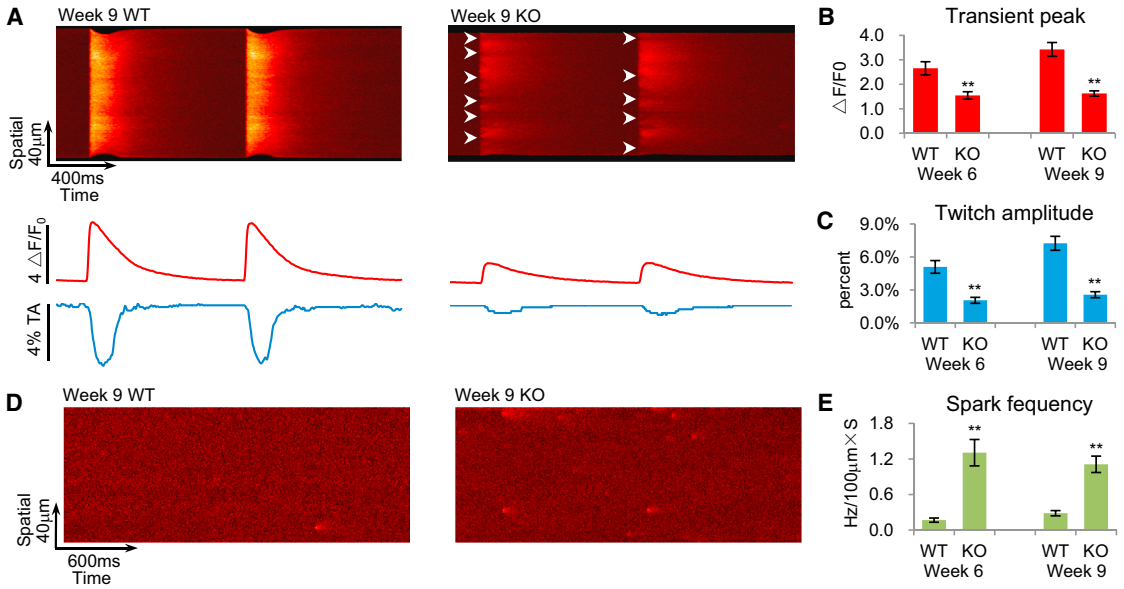

Figure 3. Defective EC Coupling in *RBFox2* KO Cardiac Muscle

(A) Confocal images of intracellular calcium transients and contraction. Isolated cardiomyocytes from WT and KO mice at 9 weeks of age were paced electrically at 1.0 Hz. Lower row shows the traces of spatially averaged calcium transient (top) and the corresponding cell shortening (bottom).

(B and C) Statistics of calcium transient peak ($\Delta F/F_0$, which is defined as the ratio between the signal and baseline) and twitch amplitude (TA) in cardiomyocytes from WT and KO mice at two different ages. The data were based on the analysis of 13–20 cells from three hearts and expressed as mean ± SEM. **$p < 0.01$.

(D) Confocal measurement of spontaneous calcium sparks in 9-week WT or KO cardiomyocytes at rest.

(E) Statistics of the frequency of calcium sparks in cardiomyocytes from WT or KO mice at two different ages. The data were based on the analysis of 14–20 cells from three hearts and expressed as mean ± SEM. **$p < 0.01$. See also Figure S2 on the results observed on RBFox2 siRNA-treated cardiomyocytes.

upstream introns and stimulated exon skipping when RBFox2 bound downstream introns (Figure 4D). In contrast, we saw no such correlation with the splicing responses additionally detected at weeks 9 and 18 (Figure 4E). These data indicate that the alternatively spliced genes recorded at week 5 are likely primary targets for RBFox2, whereas those additionally detected in later stages are secondary responses to accumulating defects in *RBFox2*$^{-/-}$ heart.

Critical Splicing Changes Underlie Specific Functional Defects in *RBFox2* KO Mice

We previously demonstrated the robustness of the RASL-seq platform in profiling alternative splicing (Zhou et al., 2012), which we further confirmed by RT-PCR on a panel of altered splicing events at three developmental ages and linked those induced-splicing to specific RBFox2-binding events (Figures 5A–5D and S4). Specific genes chosen for validation were based on their existing functional information on heart development and/or disease. For example, *Pdlim5* and *Ldb3* are important for maintaining the structural integrity of the contractile apparatus in the heart (Cheng et al., 2010; Zheng et al., 2009). RBFox2 bound multiple strong consensus motifs (red) located in the upstream intronic regions as well as on the alternative *Pdlim5* exon 5a, resulting in suppression of the alternative exon (Figure 5A). Near the alternative exon 11 in *Ldb3*, RBFox2 bound both upstream and downstream intronic regions (although these motifs were not evolutionarily conserved, labeled yellow, indicating potential synergistic actions of other RNA-binding proteins), with a net effect that led to exon skipping in *RBFox2*$^{-/-}$ heart (Figure 5B).

We further probed the protein levels by western blotting, showing reciprocal increase in the exon 5a-containing L isoform and decrease in the exon 5b-containing S isoform in the case of *Pdlim5* in response to *RBFox2* KO (Figure 5E). Note that both *Pdlim5* and *Ldb3* genes produced two alternatively polyadenylated isoforms (L and S) in which the L isoform carried both alternatively spliced mRNA isoforms, and *RBFox2* ablation induced the smaller isoform at both the RNA and protein levels (Figures 5B and 5E). The protein levels of both PDLIM5-S and LDB3-S were also progressively diminished, indicating accumulating effects in *RBFox2*$^{-/-}$ heart (Figure 5E).

We similarly validated additional RBFox2-regulated genes at week 5 and onward, including *Abcc9* (an ATP-sensitive potassium channel), *Sorbs1* and *Sorbs2* (both being SH3 domain-containing signaling molecules), and *Enah* (involved in cytoskeleton organization and remodeling), each of which showed specific RBFox2-binding events at locations that are consistent with the positional rule established for RBFox2-regulated splicing (Figure S4). Importantly, these genes also have been previously linked to DCM (Aguilar et al., 2011; Bienengraeber et al., 2004; Gehmlich et al., 2007; Yung et al., 2004).

Critical Splicing Events Were Induced in Key Transcription Factor Genes

We also observed a major impact of *RBFox2* ablation on alternative splicing of the MEF family of transcription factors,

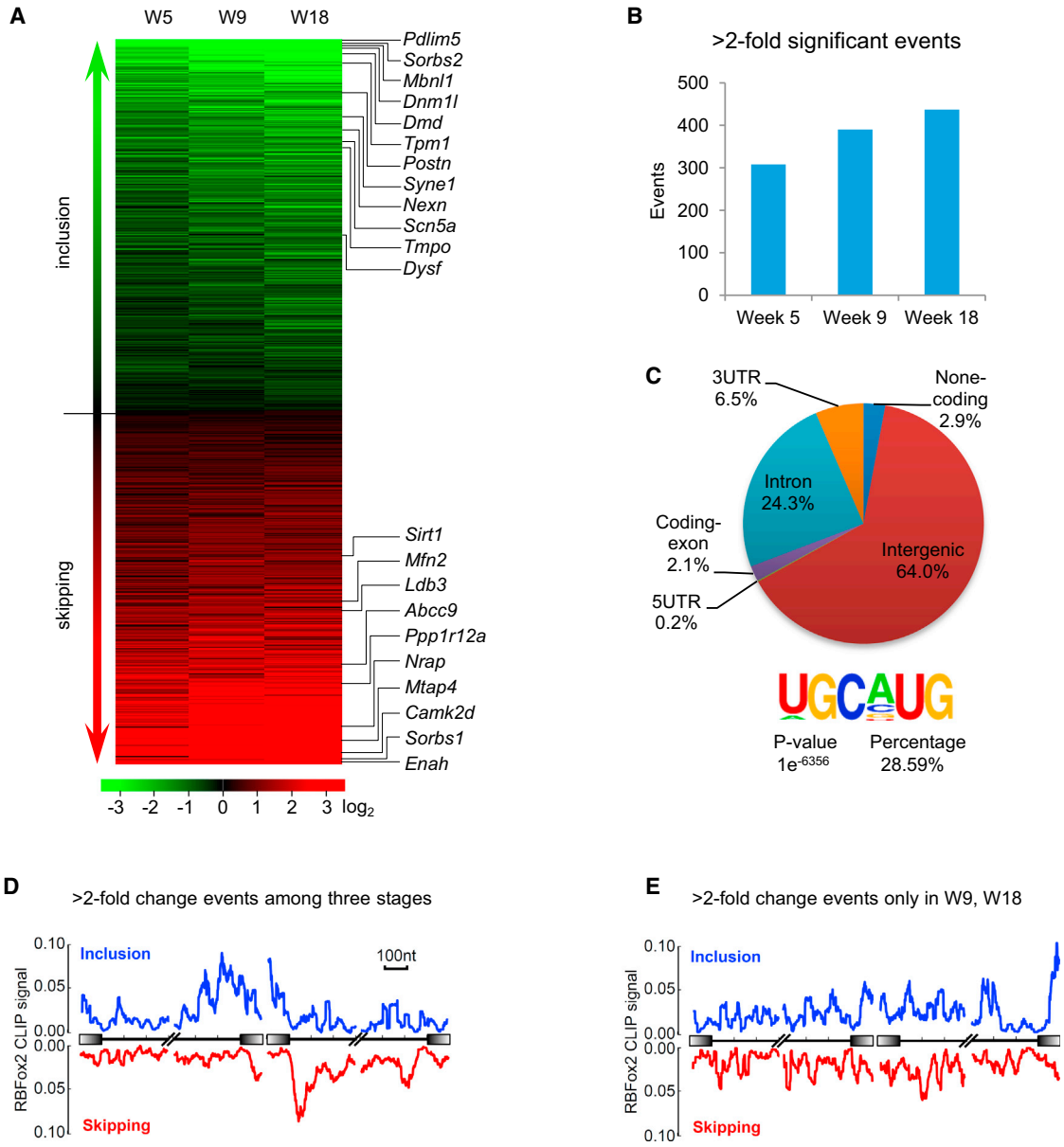

Figure 4. Primary and Accumulated Defects in Disease Progression

(A) The heatmap of the splicing profiling data by RASL-seq among three different disease stages. The data were sorted by the mean value of the three stages groups analyzed. Green, induced inclusion; red, induced skipping. Genes that previously were linked to DCM are highlighted on the right.

(B) Number of >2-fold significant events among disease stages.

(C) The genomic distribution of RBFox2 CLIP-seq reads (top). The top enriched motif and the percentage of the motif on total CLIP peaks are shown (bottom).

(D and E) The RNA maps of RBFox2-binding and -splicing responses based on those with >2-fold change relative to WT consistently detected among all three stages (D) versus changes detected only in mice at weeks 9 and 18 (E). See also Figure S3 and Table S2.

causing the exclusion of the alternative exon 9 in *Mef2a* and the alternative exon 7' in *Mef2d* (Figures 5C and S4), similar to a recent report in C2C12 cells (Singh et al., 2014). These induced isoform switches previously have been shown to affect their activities in transcription (Zhu et al., 2005), consistent with widespread changes at gene expression levels in *RBFox2* siRNA-treated C2C12 cells (Singh et al., 2014). Interestingly, while the alternative exon does not change the reading frame in both of these cases, we additionally detected a major reduction of Mef2a protein (Figure 5F), indicating the involvement of RBFox2 in additional layers of regulation. The altered transcription program may thus account for accumulating changes in alternative splicing during the development of disease phenotype in *RBFox2*$^{-/-}$ heart, as suggested for the function of RBFox1 in the nervous system (Fogel et al., 2012).

From the global perspective, we found that RBFox2-binding events are directly linked to induced alternative splicing events at week 5 (Figure 5G). Importantly, via GO term analysis of all expressed genes detected by RNA-seq (data not shown) in the mouse heart at the same developmental stage, we found that direct RBFox2 target genes are enriched in cytoskeleton organization and transcription in biological processes (Figure 5H). Together, these observations suggest that the RBFox2-regulated splicing program may directly contribute to the development of disease phenotype in *RBFox2*$^{-/-}$ heart, and many secondary effects, especially those observed in late stages, may result from induced splicing of key genes involved in transcriptional and post-transcriptional controls in cardiac muscle.

Pressure Overloading and *RBFox2* Ablation Induce a Related Splicing Program

Because TAC-induced pressure overloading diminished RBFox2, we next performed RASL-seq on sham and TAC-treated hearts, identifying 199 significantly changed splicing events (Figure S5A; Table S3). These data allowed us to compare with the splicing program in *RBFox2*$^{-/-}$ heart despite the fact that the altered splicing events in TAC-treated hearts were measured on mice at age 14 weeks (TAC treatment began at week 9 and lasted for 5 weeks), while total RNAs were extracted from *RBFox2* KO mice at postnatal week 5 after deletion of the gene in an early embryonic stage. We thus anticipated numerous compound effects to generate unique spectra of splicing changes on the two different animal models. Nonetheless, comparing between 709 splicing switches in *RBFox2*$^{-/-}$ heart and 199 events in response to TAC surgery in adult mice, we identified 76 shared events that showed an overall positive correlation between the two experimental conditions (Figure 6A, left; Table S3). Importantly, among these 76 overlapping events, 54 (71%) showed changes in the same directions (Figure 6A, right). Thus, diminished RBFox2 expression appears to partially contribute to TAC-induced splicing and heart failure.

Heart Modeling-Induced Splicing Events Are Reversed in Failing Heart

Although the identified alternative splicing events in *RBFox2*$^{-/-}$ or in TAC-treated hearts provide a rich resource for functional dissection on the single-gene basis to understand the contribution of individual altered splicing events to specific cardiac functions, the induced-splicing program as a whole is likely responsible for the complex heart failure phenotype observed on each animal model. One way to assess the global contribution of RBFox2-regulated splicing to heart failure is to compare the compendium of *RBFox2* ablation- or TAC-induced splicing events with the splicing program associated with postnatal heart remodeling. This developmentally regulated process occurs in the first month of a newborn mouse's life, and is critical for enhancing cardiac performance to meet the demand for increasing workload. In fact, multiple reprogramming events have been characterized at the level of transcription, such as switches in the expression of α to β myosine heavy chain, fetal to adult troponin I, and β to α tropomyosin (Muthuchamy et al., 1993). Importantly, switches of these genes in the reverse direction are often associated with heart failure (Krenz and Robbins, 2004; Muthuchamy et al., 1998). We thus hypothesized that the splicing program might also undergo critical reprogramming during heart remodeling.

To test this hypothesis, we performed RASL-seq on five developmental points in the first month of newborn mice from day 1 to day 28. Comparison between the two endpoints revealed 564 significant switches in alternative splicing (Figure S5B), consistent with the previous report (Giudice et al., 2014), indicating that heart remodeling in the mouse is also associated with extensive reprogramming at regulated splicing levels, which may collectively contribute to augmented heart performance. Focusing on the 54 genes that showed significantly altered splicing in the same directions between *RBFox2*$^{-/-}$ and TAC-treated hearts (Figure 6A), we found an overall negative correlation between development-associated changes and those induced by *RBFox2* ablation (Figure 6B, left; Table S3). Among these events, 36 (67%) showed changes in opposite directions (Figure 6B, right), indicating a substantial contribution of RBFox2-controlled splicing to heart remodeling.

Developmentally Regulated RBFox2 Target Genes Provide Diverse Cardiac Functions

To better appreciate the developmentally regulated splicing program relative to TAC-induced and *RBFox2* ablation-triggered splicing events, we displayed dynamic splicing changes in the 36 genes surveyed by RASL-seq at different developmental stages or under various treatment conditions (Figure 6C, green or red colors highlight induced inclusion or skipping of alternative exons). We noted that the patterns are similar between mice at day 28 and sham-operated mice at week 14, indicating that those developmentally regulated splicing events had largely completed after postnatal remodeling in the first month, and the induced mRNA isoforms then remained relatively constant in adulthood. In contrast, a large percentage of these developmentally reprogrammed splicing events were reversed in response to TAC treatment or *RBFox2* ablation (Figure 6C). This reversal strongly suggests that RBFox2-regulated splicing events contribute to augmented heart performance in adult mice.

Importantly, the majority of those developmentally regulated RBFox2 target genes (red-labeled genes on the right side of Figure 6C) have been implicated previously in heart function and/or disease. Among these genes, two (*Epb4.1*, which encodes for protein 4.1R, and *Atp5c1*, which encodes for the ATP synthetase γ subunit F1γ) have been characterized extensively as direct targets for the RBFox family of splicing regulators, and RBFox-mediated repression of the alternative exon in each case has been shown to be critical for enhanced cardiac function (Hayakawa et al., 2002; Ponthier et al., 2006). Our data now indicate that these genes are also developmentally repressed during postnatal modeling, and become derepressed in response to both TAC treatment and *RBFox2* ablation. Two other genes (*Camk2γ* and *Slc4a4*) also have been reported to respond to pressure overloading in the heart (Colomer et al., 2003; Yamamoto et al., 2007).

Other genes that show strong developmental regulation and reversal in TAC-treated and *RBFox2*-ablated mice include those involved in (1) cytoskeleton organization: *Ank1*

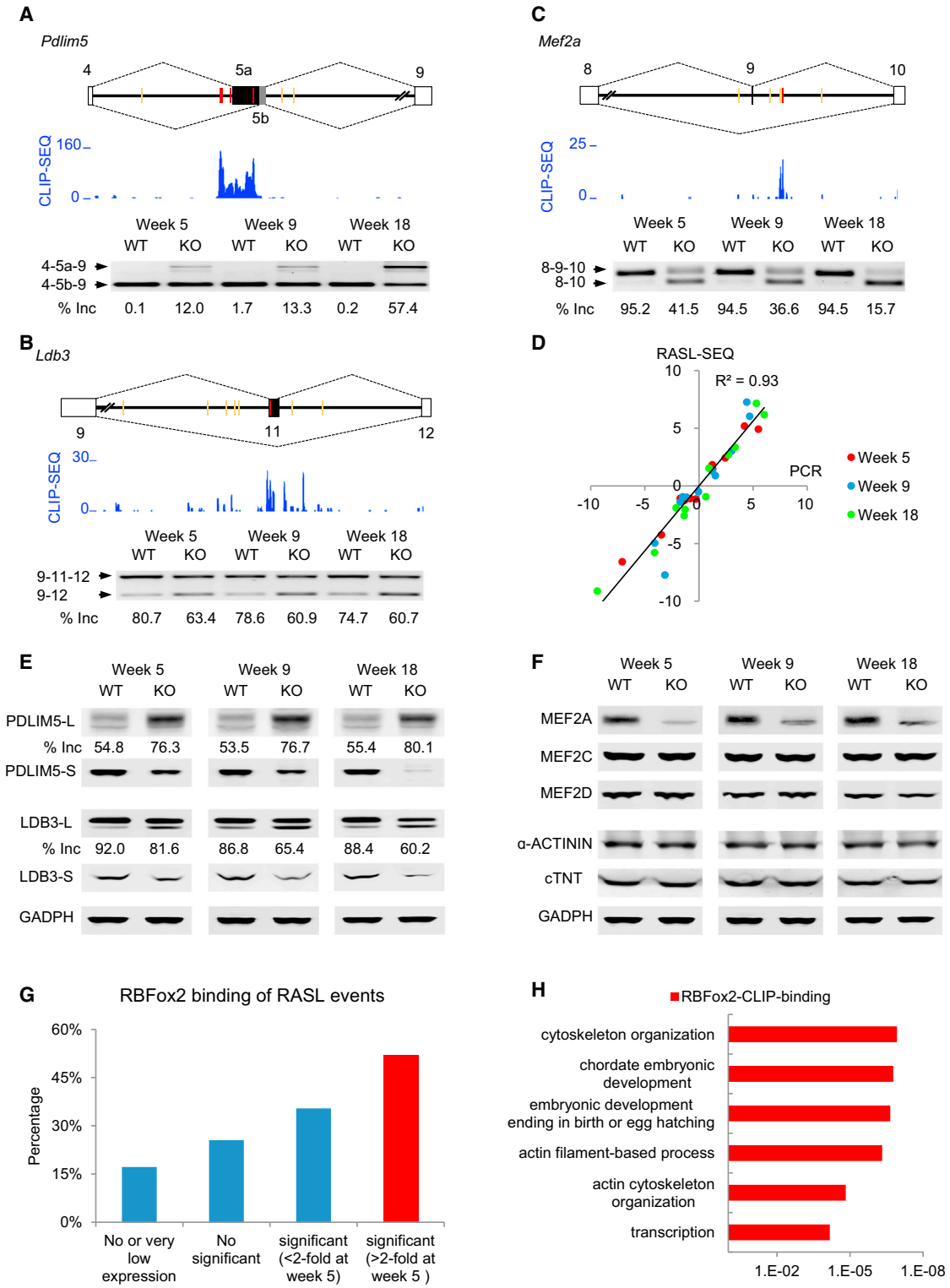

Figure 5. Critical Splicing Changes Linked to Specific Defects in the Contractile Apparatus

(A) Induced exon inclusion in *Pdlim5*. (Top) The gene structure, illustrating the alternative exon 5a and 5b. Yellow and red lines indicate the locations of non-conserved and conserved (U)GCAUG motifs, respectively. (Middle) The RBFox2 CLIP-seq signals. (Bottom) The RT-PCR results and calculated percentages of Splice-In (included exon divided by both isoforms) in each sample.

(B) Induced exon skipping in *Ldb3*. The gene structure, motif distribution, and CLIP-seq signals were similarly annotated as in (A).

(legend continued on next page)

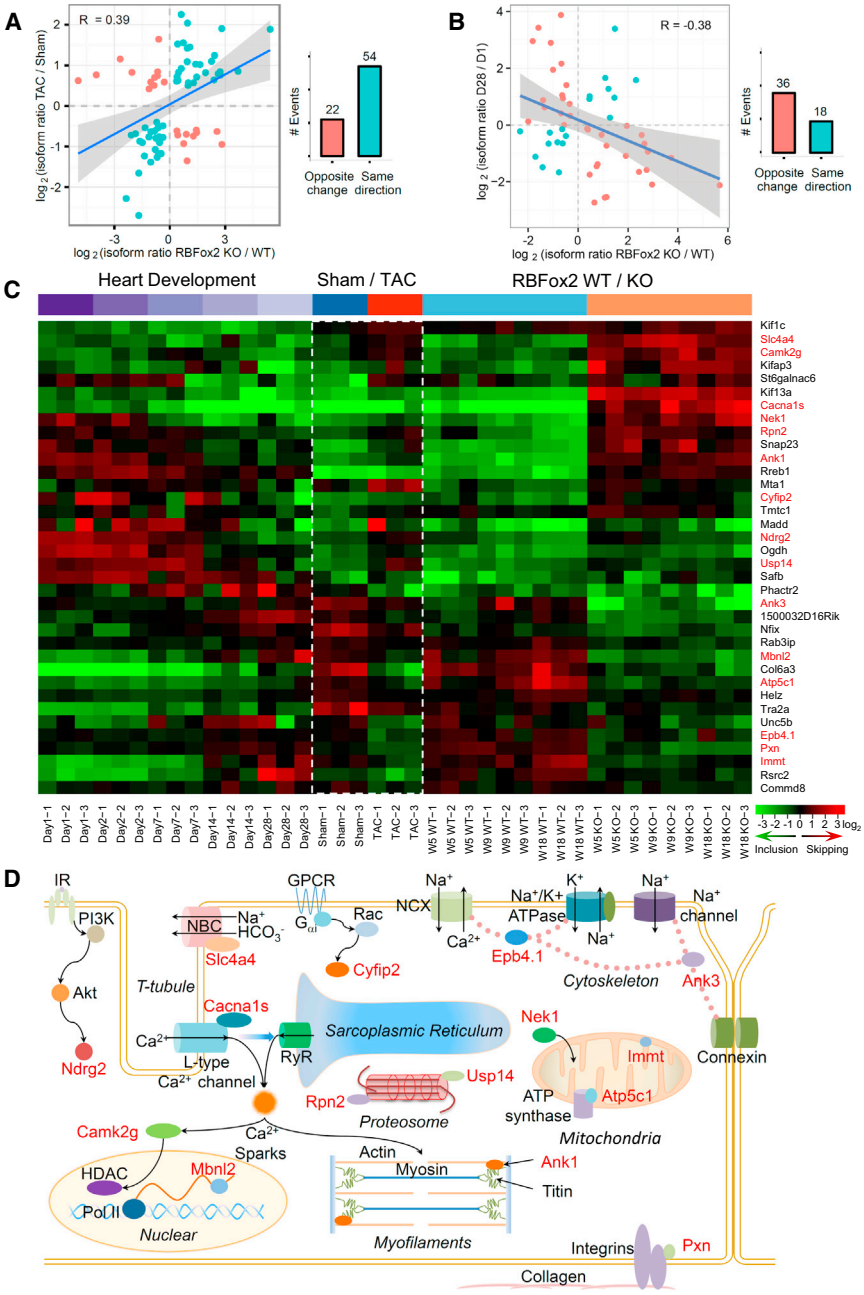

Figure 6. *RBFox2* Ablation Induces Alternative Splicing Events in the Opposite Directions during Heart Remodeling

(A) Positive correlation between significantly changed splicing events detected in response to *RBFox2* KO and TAC surgery. Green-colored dots show changes in the same directions; orange-colored dots indicate changes in the opposite directions, as summarized (right).

(B) Negative correlation between 54 events commonly induced by *RBFox2* KO and TAC and those detected during postnatal heart modeling from day 1 to day 28. Green-colored dots show changes in the same directions; orange-colored dots indicate changes in the opposite directions.

(C) Heatmap of 36 regulated splicing events that show opposite changes during heart remodeling relative to *RBFox2* KO and TAC surgery. Red-labeled on the right are genes previously implicated in heart function and/or disease.

(D) Highlight of the 15 genes (from red-labeled ones in C) with diverse regulatory functions in cardiomyocyte. IR, insulin receptor. See also Figure S5 and Table S3.

of channel activities: *Slc4a4* (Yamamoto et al., 2007) and *Cacna1s* (Stunnenberg et al., 2014); (4) proteasome functions: *Usp14* (Wilson et al., 2002) and *Rpn2* (Rosenzweig et al., 2012); (5) cellular signaling: *Pxn* (Melendez et al., 2004), *Nek1* (Chen et al., 2009), and *Cyfip2* (Schenck et al., 2003); (6) mitochondrial activities: *Immt* (Yang et al., 2012) and *Atp5c1* (Hayakawa et al., 2002); and (7) regulated splicing and translation: *Mbnl2* (Wang et al., 2012). The identification of Mbnl2 as a RBFox2 target gene exemplifies a potential cascade of regulated splicing events through RBFox2-regulated splicing regulators, given the recent observation that RBFox2 appears to function as a key regulator of splicing factors (Jangi et al., 2014). In fact, we noted that *Ndrg2*, a key gene involved in cardioprotection (Sun et al., 2013), had been reported previously to be a target gene for (Kontrogianni-Konstantopoulos and Bloch, 2003) and *Ank3* (Sato et al., 2011); (2) Ca^{2+} handling: *Epb4.1* (Stagg et al., 2008) and *Camk2γ* (Kwiatkowski and McGill, 2000); (3) regulation the Mbnl family of splicing regulators (Du et al., 2010). Together, these data suggest that RBFox2 modulates diverse regulatory functions in cardiomyocytes (Figure 6D). Although individual

(C) Induced exon skipping in *Mef2a*. The gene structure, motif distribution, and CLIP-seq signals were similarly annotated as in (A).

(D) PCR validation of 11 RASL events at three different disease stages. Black line shows the correlation of all 33 PCR results.

(E) Western blotting analysis of PDLIM5 and LDB3 in WT and KO cardiomyocytes. Note that both PDLIM5 and LDB3 have long and short isoforms resulting from alternative polyadenylation. In both cases, the long isoform contains the alternatively spliced products. The percentages of exon inclusion are based on the intensity of protein isoforms on the gel. The results had been repeated on different sets of WT and KO hearts.

(F) Western blotting analysis of multiple MEF2 family proteins; α-ACTININ and c-TNT served as the loading controls.

(G) Percentage of directly RBFox2-binding events in different RASL-seq data groups.

(H) Gene ontology analysis of direct RBFox2 target genes in biological processes based on the DAVID database. See also Figure S4.

mRNA isoforms of these genes remain to be functionally characterized, it is likely that the reversal of these developmentally regulated splicing programs may collectively contribute to heart failure in TAC-treated and *RBFox2* KO mice.

DISCUSSION

RBFox2 Controls a Large Splicing Program in the Heart

RBFox2 has emerged as a key tissue-specific regulator of alternative splicing in development and disease through recognizing the conserved UGCAUG motif in metazoans (Zhang et al., 2008). In mammalian heart, RBFox2 is expressed in a relatively constant fashion, in contrast to the dramatic induction of the related RBFox1 protein after birth (Kalsotra et al., 2008), which may together regulate and maintain a key splicing program functionally important for postnatal heart remodeling. Such a synergistic function between RBFox1 and RBFox2 has been demonstrated in zebrafish heart development (Gallagher et al., 2011). Intriguingly, RBFox2 appears to play a more important role than RBFox1 in C2C12 cells (Singh et al., 2014), and the lethal phenotype observed in *RBFox2*-ablated mice clearly demonstrated its unique contribution to cardiac function, which is consistent with the large altered splicing program in *RBFox2* KO cardiomyocytes, despite the continuous presence of RBFox1.

It is interesting to note that *RBFox2*-ablated mice were relatively morphologically normal until 5 weeks after birth, indicating that RBFox2 is critical for heart performance. By splicing profiling, we identified a large number of RBFox2 target genes based on direct binding evidence and resultant RNA map that shows the anticipated positional effects. Importantly, these RBFox2 target genes provide diverse cardiac functions, ranging from key components of the contractile apparatus to various ion channels and signaling molecules critical for coupling between excitation and contraction to genes involved in energy metabolism, as highlighted in Figure 6D. The RBFox2-regulated splicing program is likely further amplified via its immediate target genes, which include the MEF family of muscle-specific transcription factors and other critical splicing regulators (such as Mbnl2), eventually causing mortality of *RBFox2* KO mice.

RBFox2 May Serve as a Key Sensor to Stress Signaling

Our current targeting study is of physiological relevance because of the link between diminished RBFox2 protein and pressure overloading. This implicates RBFox2 as a key sensor to stress signaling in the heart. Interestingly, its mRNA level appeared unaltered, as evidenced by multiple probe signals in our RASL-seq oligonucleotide pool that remained unchanged in TAC-treated mice. This suggests that RBFox2 protein might be downregulated via a post-translational mechanism(s), which is the subject of future studies. Such unaltered mRNA would escape the detection in previous gene expression profiling experiments on animal models (Zhao et al., 2004) or human patient samples (Kaynak et al., 2003). Unfortunately, such unstable protein in TAC-treated mice discouraged us from further evaluating RBFox2 reduction and TAC-induced phenotype with a transgene.

Although it is currently unclear about the mechanism needed to trigger the reduction of RBFox2 protein in TAC-treated mice, the proposed sensor function raises an intriguing possibility that RBFox2 might be a key target in certain stress-signaling pathways. In fact, diverse signal transduction pathways have been shown to accompany physiological heart modeling or pathological responses in failing heart (van Berlo et al., 2013). Therefore, it will be an important topic for future studies to understand how RBFox2 expression is diminished in response to a specific stress signal(s). As its mRNA appeared unaltered in TAC-treated heart, it will be particularly interesting to determine whether RBFox2 is a target for a pressure overload-induced microRNA (Reddy et al., 2012). Proteasome-mediated degradation also remains a formal possibility to be tested in future investigation.

RBFox2 Might Be a Key Component of Decompensation in Failing Heart

Mammalian genomes encode for a large number of RNA-binding proteins, which together control an extensive alternative splicing program (Fu and Ares, 2014) in development and disease (Kalsotra and Cooper, 2011). Because alternative splicing often introduces subtle changes in mRNA that may alter RNA stability and/or function, it has remained a major challenge to infer functional consequences among numerous altered splicing events in a given cell type or biological system. Here, we took advantage of postnatal heart remodeling, a well-known positive force for augmentation of cardiac functions. By profiling splicing in this critical developmental window, we identified a set of alternative splicing events that are switched in a monotonic fashion. Importantly, many of those events were reversed in response to TAC treatment or *RBFox2* ablation, thus consistent with comprised cardiac function via such a regulated splicing program. This includes F1γ (encoded by *Atp5c1*), one of the best biochemically characterized RBFox2 target genes (Fukumura et al., 2007), and splicing of this ATP synthetase gene is known to enhance energy production in the mitochondria of cardiac muscle (Hayakawa et al., 2002). Defects in this and other RBFox2 target genes may thus collectively contribute to heart failure in *RBFox2* KO mice.

Our functional study of RBFox2-regulated splicing on the mouse model also provides critical insights into cardiac decompensation, which is a key but poorly understood process during heart failure. We found that *RBFox2* ablation induced a failure phenotype without first inducing cardiac hypertrophy, consistent with other genetic models in which compensation and decompensation appear decoupled (Diwan and Dorn, 2007). Our observations, that TAC triggered a dramatic reduction in RBFox2 expression and both TAC and RBFox2 ablation produced related disease phenotypes and regulated a set of key alternative splicing events, strongly suggest that RBFox2 may be a key component of cardiac decompensation. It will be of great interest to determine in future studies whether the RBFox2 level could be correlated to hypertension-induced cardiac malfunction in humans.

EXPERIMENTAL PROCEDURES

All works on animals were performed according to the protocol (S99116) approved by our institutional review board.

Transaortic Banding Surgery

Nine-week-old male littermate mice were subjected to pressure overload by TAC surgery, as described previously (Guo et al., 2014). After 5 weeks

postsurgery, total protein and RNA were extracted from isolated cardiomyocytes from sham and TAC-treated mice for western blotting, RASL-seq, and RT-PCR.

Generation of *RBFox2* Cardiac-Specific KO Mice

The construction of conditional *RBFox2* KO mice has been described previously (Gehman et al., 2012). Crossing of the mice with the *Mlc2v-Cre* transgenic mouse and characterization of the mutant mice are detailed in the Supplemental Experimental Procedures. Specific siRNAs used in the current study are listed in Table S1.

Echocardiography and Calcium Imaging

Phenotypic and echocardiographic analyses of *RBFox2*-ablated heart were performed according to Xu and Fu (2005), and details also are provided in the Supplemental Experimental Procedures.

RASL-Seq Profiling, Data Analysis, and RT-PCR Validation

RASL-seq is designed to profile mRNA isoforms using pooled pairs of oligonucleotides each flanked by a universal primer to target specific splice junctions in spliced mRNAs, as previously described (Li et al., 2012), and are detailed in the Supplemental Experimental Procedures. Significantly changed splicing events at different developmental stages in *RBFox2* KO mice over WT are listed in Table S2, and those induced by TAC treatment over sham operation and those altered during postnatal heart development are listed in Table S3.

RBFox2 CLIP-Seq

RBFox2 CLIP-seq and construction of the RBFox2 RNA map were detailed previously (Yeo et al., 2009). A rabbit polyclonal anti-RBFox2 antibody (Bethyl Laboratories, A300-864A) was used to immunoprecipitate RBFox2-RNA complexes from isolated cardiomyocytes of week 9 mice hearts. For detailed analyses, see the data analysis in the Supplemental Experimental Procedures.

ACCESSION NUMBERS

The RASL-seq, RNA-seq, and CLIP-seq data presented in this report have been deposited to the NCBI GEO and are available under the accession number GSE57926.

SUPPLEMENTAL INFORMATION

Supplemental Information includes Supplemental Experimental Procedures, five figures, and three tables and can be found with this article online at http://dx.doi.org/10.1016/j.celrep.2015.02.013.

AUTHOR CONTRIBUTIONS

C.W and X.-D.F designed the experiments. C.W. generated the KO mouse and carried out molecular and phenotypic analysis with assistance from K.O. and I.B. J.Q. performed splicing profiling by RASL-seq. Y.Z., C.W., and J.Q. analyzed the data. Y.X. and J.H. performed CLIP-seq. H.L. was responsible for deep sequencing. C.Z performed pressure-overloading experiments. J.C., L.-S.S., and X.-D.F. guided experimental design and data interpretation. C.W. and X.-D.F. wrote the paper.

ACKNOWLEDGMENTS

The authors are grateful to members of the X.-D.F. lab for cooperation, reagent sharing, and stimulating discussion during the course of this investigation. This work was supported by NIH grants (GM049369, HG004659, and HG007005) to X.-D.F.

Received: September 12, 2014
Revised: November 2, 2014
Accepted: January 31, 2015
Published: March 5, 2015

REFERENCES

Aguilar, F., Belmonte, S.L., Ram, R., Noujaim, S.F., Dunaevsky, O., Protack, T.L., Jalife, J., Todd Massey, H., Gertler, F.B., and Blaxall, B.C. (2011). Mammalian enabled (Mena) is a critical regulator of cardiac function. Am. J. Physiol. Heart Circ. Physiol. *300*, H1841–H1852.

Bienengraeber, M., Olson, T.M., Selivanov, V.A., Kathmann, E.C., O'Cochlain, F., Gao, F., Karger, A.B., Ballew, J.D., Hodgson, D.M., Zingman, L.V., et al. (2004). ABCC9 mutations identified in human dilated cardiomyopathy disrupt catalytic KATP channel gating. Nat. Genet. *36*, 382–387.

Chen, J., Kubalak, S.W., and Chien, K.R. (1998). Ventricular muscle-restricted targeting of the RXRalpha gene reveals a non-cell-autonomous requirement in cardiac chamber morphogenesis. Development *125*, 1943–1949.

Chen, Y., Craigen, W.J., and Riley, D.J. (2009). Nek1 regulates cell death and mitochondrial membrane permeability through phosphorylation of VDAC1. Cell Cycle *8*, 257–267.

Cheng, H., and Lederer, W.J. (2008). Calcium sparks. Physiol. Rev. *88*, 1491–1545.

Cheng, H., Kimura, K., Peter, A.K., Cui, L., Ouyang, K., Shen, T., Liu, Y., Gu, Y., Dalton, N.D., Evans, S.M., et al. (2010). Loss of enigma homolog protein results in dilated cardiomyopathy. Circ. Res. *107*, 348–356.

Colomer, J.M., Mao, L., Rockman, H.A., and Means, A.R. (2003). Pressure overload selectively up-regulates Ca2+/calmodulin-dependent protein kinase II in vivo. Mol. Endocrinol. *17*, 183–192.

Diwan, A., and Dorn, G.W., 2nd. (2007). Decompensation of cardiac hypertrophy: cellular mechanisms and novel therapeutic targets. Physiology (Bethesda) *22*, 56–64.

Du, H., Cline, M.S., Osborne, R.J., Tuttle, D.L., Clark, T.A., Donohue, J.P., Hall, M.P., Shiue, L., Swanson, M.S., Thornton, C.A., and Ares, M., Jr. (2010). Aberrant alternative splicing and extracellular matrix gene expression in mouse models of myotonic dystrophy. Nat. Struct. Mol. Biol. *17*, 187–193.

Fogel, B.L., Wexler, E., Wahnich, A., Friedrich, T., Vijayendran, C., Gao, F., Parikshak, N., Konopka, G., and Geschwind, D.H. (2012). RBFOX1 regulates both splicing and transcriptional networks in human neuronal development. Hum. Mol. Genet. *21*, 4171–4186.

Fu, X.D., and Ares, M., Jr. (2014). Context-dependent control of alternative splicing by RNA-binding proteins. Nat. Rev. Genet. *15*, 689–701.

Fukumura, K., Kato, A., Jin, Y., Ideue, T., Hirose, T., Kataoka, N., Fujiwara, T., Sakamoto, H., and Inoue, K. (2007). Tissue-specific splicing regulator Fox-1 induces exon skipping by interfering E complex formation on the downstream intron of human F1gamma gene. Nucleic Acids Res. *35*, 5303–5311.

Gallagher, T.L., Arribere, J.A., Geurts, P.A., Exner, C.R., McDonald, K.L., Dill, K.K., Marr, H.L., Adkar, S.S., Garnett, A.T., Amacher, S.L., and Conboy, J.G. (2011). Rbfox-regulated alternative splicing is critical for zebrafish cardiac and skeletal muscle functions. Dev. Biol. *359*, 251–261.

Gehman, L.T., Stoilov, P., Maguire, J., Damianov, A., Lin, C.H., Shiue, L., Ares, M., Jr., Mody, I., and Black, D.L. (2011). The splicing regulator Rbfox1 (A2BP1) controls neuronal excitation in the mammalian brain. Nat. Genet. *43*, 706–711.

Gehman, L.T., Meera, P., Stoilov, P., Shiue, L., O'Brien, J.E., Meisler, M.H., Ares, M., Jr., Otis, T.S., and Black, D.L. (2012). The splicing regulator Rbfox2 is required for both cerebellar development and mature motor function. Genes Dev. *26*, 445–460.

Gehmlich, K., Pinotsis, N., Hayess, K., van der Ven, P.F., Milting, H., El Banayosy, A., Körfer, R., Wilmanns, M., Ehler, E., and Fürst, D.O. (2007). Paxillin and ponsin interact in nascent costameres of muscle cells. J. Mol. Biol. *369*, 665–682.

Giudice, J., Xia, Z., Wang, E.T., Scavuzzo, M.A., Ward, A.J., Kalsotra, A., Wang, W., Wehrens, X.H., Burge, C.B., Li, W., and Cooper, T.A. (2014). Alternative splicing regulates vesicular trafficking genes in cardiomyocytes during postnatal heart development. Nat. Commun. *5*, 3603.

Guo, A., Zhang, X., Iyer, V.R., Chen, B., Zhang, C., Kutschke, W.J., Weiss, R.M., Franzini-Armstrong, C., and Song, L.S. (2014). Overexpression of

junctophilin-2 does not enhance baseline function but attenuates heart failure development after cardiac stress. Proc. Natl. Acad. Sci. USA *111*, 12240–12245.

Hayakawa, M., Sakashita, E., Ueno, E., Tominaga, S., Hamamoto, T., Kagawa, Y., and Endo, H. (2002). Muscle-specific exonic splicing silencer for exon exclusion in human ATP synthase gamma-subunit pre-mRNA. J. Biol. Chem. *277*, 6974–6984.

Hill, J.A., Karimi, M., Kutschke, W., Davisson, R.L., Zimmerman, K., Wang, Z., Kerber, R.E., and Weiss, R.M. (2000). Cardiac hypertrophy is not a required compensatory response to short-term pressure overload. Circulation *101*, 2863–2869.

Jangi, M., Boutz, P.L., Paul, P., and Sharp, P.A. (2014). Rbfox2 controls autoregulation in RNA-binding protein networks. Genes Dev. *28*, 637–651.

Kalsotra, A., and Cooper, T.A. (2011). Functional consequences of developmentally regulated alternative splicing. Nat. Rev. Genet. *12*, 715–729.

Kalsotra, A., Xiao, X., Ward, A.J., Castle, J.C., Johnson, J.M., Burge, C.B., and Cooper, T.A. (2008). A postnatal switch of CELF and MBNL proteins reprograms alternative splicing in the developing heart. Proc. Natl. Acad. Sci. USA *105*, 20333–20338.

Kaynak, B., von Heydebreck, A., Mebus, S., Seelow, D., Hennig, S., Vogel, J., Sperling, H.P., Pregla, R., Alexi-Meskishvili, V., Hetzer, R., et al. (2003). Genome-wide array analysis of normal and malformed human hearts. Circulation *107*, 2467–2474.

Kim, K.K., Adelstein, R.S., and Kawamoto, S. (2009). Identification of neuronal nuclei (NeuN) as Fox-3, a new member of the Fox-1 gene family of splicing factors. J. Biol. Chem. *284*, 31052–31061.

Kontrogianni-Konstantopoulos, A., and Bloch, R.J. (2003). The hydrophilic domain of small ankyrin-1 interacts with the two N-terminal immunoglobulin domains of titin. J. Biol. Chem. *278*, 3985–3991.

Krenz, M., and Robbins, J. (2004). Impact of beta-myosin heavy chain expression on cardiac function during stress. J. Am. Coll. Cardiol. *44*, 2390–2397.

Kuroyanagi, H. (2009). Fox-1 family of RNA-binding proteins. Cell. Mol. Life Sci. *66*, 3895–3907.

Kwiatkowski, A.P., and McGill, J.M. (2000). Alternative splice variant of gamma-calmodulin-dependent protein kinase II alters activation by calmodulin. Arch. Biochem. Biophys. *378*, 377–383.

Li, H., Qiu, J., and Fu, X.D. (2012). RASL-seq for massively parallel and quantitative analysis of gene expression. Curr. Protoc. Mol. Biol. *Chapter 4*, 1–9.

Marber, M.S., Rose, B., and Wang, Y. (2011). The p38 mitogen-activated protein kinase pathway—a potential target for intervention in infarction, hypertrophy, and heart failure. J. Mol. Cell. Cardiol. *51*, 485–490.

Melendez, J., Turner, C., Avraham, H., Steinberg, S.F., Schaefer, E., and Sussman, M.A. (2004). Cardiomyocyte apoptosis triggered by RAFTK/pyk2 via Src kinase is antagonized by paxillin. J. Biol. Chem. *279*, 53516–53523.

Muthuchamy, M., Pajak, L., Howles, P., Doetschman, T., and Wieczorek, D.F. (1993). Developmental analysis of tropomyosin gene expression in embryonic stem cells and mouse embryos. Mol. Cell. Biol. *13*, 3311–3323.

Muthuchamy, M., Boivin, G.P., Grupp, I.L., and Wieczorek, D.F. (1998). Beta-tropomyosin overexpression induces severe cardiac abnormalities. J. Mol. Cell. Cardiol. *30*, 1545–1557.

Ponthier, J.L., Schluepen, C., Chen, W., Lersch, R.A., Gee, S.L., Hou, V.C., Lo, A.J., Short, S.A., Chasis, J.A., Winkelmann, J.C., and Conboy, J.G. (2006). Fox-2 splicing factor binds to a conserved intron motif to promote inclusion of protein 4.1R alternative exon 16. J. Biol. Chem. *281*, 12468–12474.

Reddy, S., Zhao, M., Hu, D.Q., Fajardo, G., Hu, S., Ghosh, Z., Rajagopalan, V., Wu, J.C., and Bernstein, D. (2012). Dynamic microRNA expression during the transition from right ventricular hypertrophy to failure. Physiol. Genomics *44*, 562–575.

Rosenzweig, R., Bronner, V., Zhang, D., Fushman, D., and Glickman, M.H. (2012). Rpn1 and Rpn2 coordinate ubiquitin processing factors at proteasome. J. Biol. Chem. *287*, 14659–14671.

Sato, P.Y., Coombs, W., Lin, X., Nekrasova, O., Green, K.J., Isom, L.L., Taffet, S.M., and Delmar, M. (2011). Interactions between ankyrin-G, Plakophilin-2, and Connexin43 at the cardiac intercalated disc. Circ. Res. *109*, 193–201.

Schenck, A., Bardoni, B., Langmann, C., Harden, N., Mandel, J.L., and Giangrande, A. (2003). CYFIP/Sra-1 controls neuronal connectivity in Drosophila and links the Rac1 GTPase pathway to the fragile X protein. Neuron *38*, 887–898.

Sebat, J., Lakshmi, B., Malhotra, D., Troge, J., Lese-Martin, C., Walsh, T., Yamrom, B., Yoon, S., Krasnitz, A., Kendall, J., et al. (2007). Strong association of de novo copy number mutations with autism. Science *316*, 445–449.

Singh, R.K., Xia, Z., Bland, C.S., Kalsotra, A., Scavuzzo, M.A., Curk, T., Ule, J., Li, W., and Cooper, T.A. (2014). Rbfox2-coordinated alternative splicing of Mef2d and Rock2 controls myoblast fusion during myogenesis. Mol. Cell *55*, 592–603.

Stagg, M.A., Carter, E., Sohrabi, N., Siedlecka, U., Soppa, G.K., Mead, F., Mohandas, N., Taylor-Harris, P., Baines, A., Bennett, P., et al. (2008). Cytoskeletal protein 4.1R affects repolarization and regulates calcium handling in the heart. Circ. Res. *103*, 855–863.

Stunnenberg, B.C., Deinum, J., Links, T.P., Wilde, A.A., Franssen, H., and Drost, G. (2014). Cardiac arrhythmias in hypokalemic periodic paralysis: Hypokalemia as only cause? Muscle Nerve *50*, 327–332.

Sun, Z., Tong, G., Ma, N., Li, J., Li, X., Li, S., Zhou, J., Xiong, L., Cao, F., Yao, L., et al. (2013). NDRG2: a newly identified mediator of insulin cardioprotection against myocardial ischemia-reperfusion injury. Basic Res. Cardiol. *108*, 341.

van Berlo, J.H., Maillet, M., and Molkentin, J.D. (2013). Signaling effectors underlying pathologic growth and remodeling of the heart. J. Clin. Invest. *123*, 37–45.

Venables, J.P., Klinck, R., Koh, C., Gervais-Bird, J., Bramard, A., Inkel, L., Durand, M., Couture, S., Froehlich, U., Lapointe, E., et al. (2009). Cancer-associated regulation of alternative splicing. Nat. Struct. Mol. Biol. *16*, 670–676.

Wang, E.T., Cody, N.A., Jog, S., Biancolella, M., Wang, T.T., Treacy, D.J., Luo, S., Schroth, G.P., Housman, D.E., Reddy, S., et al. (2012). Transcriptome-wide regulation of pre-mRNA splicing and mRNA localization by muscleblind proteins. Cell *150*, 710–724.

Wilson, S.M., Bhattacharyya, B., Rachel, R.A., Coppola, V., Tessarollo, L., Householder, D.B., Fletcher, C.F., Miller, R.J., Copeland, N.G., and Jenkins, N.A. (2002). Synaptic defects in ataxia mice result from a mutation in Usp14, encoding a ubiquitin-specific protease. Nat. Genet. *32*, 420–425.

Xu, X., and Fu, X.D. (2005). Conditional knockout mice to study alternative splicing in vivo. Methods *37*, 387–392.

Yamamoto, T., Shirayama, T., Sakatani, T., Takahashi, T., Tanaka, H., Takamatsu, T., Spitzer, K.W., and Matsubara, H. (2007). Enhanced activity of ventricular Na+-HCO3- cotransport in pressure overload hypertrophy. Am. J. Physiol. Heart Circ. Physiol. *293*, H1254–H1264.

Yang, R.F., Zhao, G.W., Liang, S.T., Zhang, Y., Sun, L.H., Chen, H.Z., and Liu, D.P. (2012). Mitofilin regulates cytochrome c release during apoptosis by controlling mitochondrial cristae remodeling. Biochem. Biophys. Res. Commun. *428*, 93–98.

Yeo, G.W., Coufal, N.G., Liang, T.Y., Peng, G.E., Fu, X.D., and Gage, F.H. (2009). An RNA code for the FOX2 splicing regulator revealed by mapping RNA-protein interactions in stem cells. Nat. Struct. Mol. Biol. *16*, 130–137.

Yung, C.K., Halperin, V.L., Tomaselli, G.F., and Winslow, R.L. (2004). Gene expression profiles in end-stage human idiopathic dilated cardiomyopathy: altered expression of apoptotic and cytoskeletal genes. Genomics *83*, 281–297.

Zhang, C., Zhang, Z., Castle, J., Sun, S., Johnson, J., Krainer, A.R., and Zhang, M.Q. (2008). Defining the regulatory network of the tissue-specific splicing factors Fox-1 and Fox-2. Genes Dev. *22*, 2550–2563.

Zhao, M., Chow, A., Powers, J., Fajardo, G., and Bernstein, D. (2004). Microarray analysis of gene expression after transverse aortic constriction in mice. Physiol. Genomics *19*, 93–105.

Zheng, M., Cheng, H., Li, X., Zhang, J., Cui, L., Ouyang, K., Han, L., Zhao, T., Gu, Y., Dalton, N.D., et al. (2009). Cardiac-specific ablation of Cypher leads to a severe form of dilated cardiomyopathy with premature death. Hum. Mol. Genet. *18*, 701–713.

Zhou, Z., Qiu, J., Liu, W., Zhou, Y., Plocinik, R.M., Li, H., Hu, Q., Ghosh, G., Adams, J.A., Rosenfeld, M.G., and Fu, X.D. (2012). The Akt-SRPK-SR axis constitutes a major pathway in transducing EGF signaling to regulate alternative splicing in the nucleus. Mol. Cell *47*, 422–433.

Zhu, B., Ramachandran, B., and Gulick, T. (2005). Alternative pre-mRNA splicing governs expression of a conserved acidic transactivation domain in myocyte enhancer factor 2 factors of striated muscle and brain. J. Biol. Chem. *280*, 28749–28760.